Stochastic Resonance Crossovers in Complex Networks

Giovanni Pinamonti[¤], J. Marro, Joaquín J. Torres*

Institute "Carlos I" for Theoretical and Computational Physics, and Department of Electromagnetism and Matter Physics, University of Granada, Granada, Spain

Abstract

Here we numerically study the emergence of stochastic resonance as a mild phenomenon and how this transforms into an amazing enhancement of the signal-to-noise ratio at several levels of a disturbing ambient noise. The setting is a cooperative, interacting complex system modelled as an Ising-Hopfield network in which the intensity of mutual interactions or "synapses" varies with time in such a way that it accounts for, e.g., a kind of fatigue reported to occur in the cortex. This induces *nonequilibrium* phase transitions whose rising comes associated to various mechanisms producing two types of resonance. The model thus clarifies the details of the signal transmission and the causes of correlation among noise and signal. We also describe short-time persistent memory states, and conclude on the limited relevance of the network wiring topology. Our results, in qualitative agreement with the observation of excellent transmission of weak signals in the brain when competing with both intrinsic and external noise, are expected to be of wide validity and may have technological application. We also present here a first contact between the model behavior and psychotechnical data.

Introduction

Ambient fluctuations that are treated as annoying and often ignored play in fact a fundamental role in nature. For example, they may transmit information notwithstanding their deceptive lack of structure (see, e.g., [1,2]), help setting up order at the macroscopic, mesoscopic and even nanoscopic levels despite their apparent order-disturbing effect [3], and optimize propagation by turning the medium into an excitable one [4,5] and inducing coherence among environmental noise and the periodic part of the signal, which helps weak inputs to go through without damping. This is named *stochastic resonance* (SR) which, believed to occur in many different instances [6–15], and known to be technologically relevant, e.g., in designing filters and sensory devices and in extracting details about waves-traversed geological media [16,17], is now established as a genuine and common, perhaps universal phenomenon [18–20].

Deciphering the detailed microscopic mechanisms bringing a constructive role of diverse fluctuations in such a varied range of circumstances is puzzling. This goal became even more difficult after the discovery of *stochastic multi-resonance* (SMR) in human perception [21] in accordance with predictions in assorted contexts, which demands searching for further causes [22–27]. The hallmark of SR is a rise of the power spectral density or the input-output correlation with increasing strength of a noise which is competing with the main input signal. The noise tends again to dominate, so that the signal transmission may be impeded in practice, past a peak as the noise level is further increased. One speaks of SMR when several peaks of this kind show up for different levels of noise.

In this paper, we report on a numerical study of SR and SMR in the Ising system on a network in which each node is linked to each other. Such a full wiring is not realistic but this feature is in practice swept away here by assuming inhomogeneous connectivity. That is, the interactions or connections are weighted and time varying following a pattern which has been observed, for instance, in the central nervous system [28–31]. This transforms in practice the original regular net into an effective complex network whose links happen to play an essential role, as described in detail, for example, in [31] and references therein. The ambient noise is modelled in our case by the standard thermal bath, and an external deterministic, time-periodic signal is added to the current arriving each unit. Using this simple setting, in which one may think of units and connections as oversimplified neurons and synapses, respectively, we describe a crossover from SR to SMR by changing the dynamic properties of synapses. Important features of SMR phenomena are then tuned by simply modifying model parameters that have a well-defined physical meaning. Our study thus deepens on the microscopic basis and therefore on the detailed nature of SMR as it may occur in an ample family of complex, cooperative or interacting systems, and we relate SMR to nonequilibrium phase transitions that are known to bear relevance to the understanding of some brain functions [32,33].

Methods

Let N binary neurons, namely, $s_i = 0$ or 1, $i = 1,...,N$, each linked to the rest by synapses $i \leftrightarrow j = 1,...,N$, whose intensities or weights are given by the *covariance rule* [34]:

$$\omega_{ij} = \frac{1}{Np(1-p)} \sum_{\mu} \left(\xi_i^{\mu} - p\right)\left(\xi_j^{\mu} - p\right), \quad \omega_{ii} = 0. \qquad (1)$$

This, which modifies the familiar Hebbian prescription to avoid saturation of weights, as if there were a threshold, involves P patterns, namely, $\{\xi_i^{\mu} = 0,1\}$ with $\mu = 1,\ldots,P$, that are assumed to have been previously "learned" by the system. The parameter p in (1) measures the excess of 1's over 0's or symmetry in the mean net activity of the set of patterns, namely, $p = \langle \xi_i^{\mu} \rangle_{i,\mu}$. In practice, for simplicity and also to avoid specificities concerning this model feature, we deal here with random patterns in the sense that each ξ_i^{μ} is given either 0 or 1 at random with the only restriction that $\langle \xi_i^{\mu} \rangle_{i,\mu}$ equals the given value of p.

Evolution with time is by parallel, cellular automata dynamics, namely, by stochastic changes at each time of the whole set $\mathbf{s} = \{s_i\}$ according to the probabilities:

$$P_i\{s_i(t+1) = \sigma\} = \frac{1}{2} + \left(\sigma - \frac{1}{2}\right)\tanh\left[I_i(t)T^{-1}\right], \forall i. \qquad (2)$$

Here, σ equals either 1 or 0, T is the temperature of the underlaying bath, and

$$I_i(t) = 2[h_i(t) - \theta_i + A(t)] \qquad (3)$$

stands for the total input on each neuron. The last term in this equation is an external signal that we shall first assume to be $A(t) = A_0 \cos(ft)$ (see, however, the section "Changing the signal" below) where the amplitude A_0 will in practice be small compared to the total input, and θ_i are thresholds for firing, which we take here equal to half the sum of the weights of all the synapsis connecting i to the other neurons, $\theta_i = \frac{1}{2}\sum_{j=1}^{N}\omega_{ij}$. The first term in the rhs of Eq. (3) is the net current from others on neuron i, which is given by

$$h_i(t) = \sum_{j=1}^{N} \omega_{ij} x_j(t) s_j(t). \qquad (4)$$

Therefore, we modulate the synaptic weights with the variable $x_i(t)$ that we shall assume to change with time according to the map [28]:

$$x_i(t+1) = x_i(t) + \frac{1 - x_i(t)}{\alpha} - \beta x_i(t)s_i(t). \qquad (5)$$

This ansatz could be replaced by direct assumptions on the net links that have an easy interpretation on physical grounds, see e.g. [31], without affecting our main results here. Nevertheless, the choice (5) is simpler and has been previously tested in neuroscience studies [35]. It amounts to assume a sawtooth–shaped time change, with α and β measuring the teeth width and depth, respectively, describing a competition of effects associated to synapses "fatigue". That is, the link of intensity $\omega_{ij}x_j$ is debilitated as β is increased, while decreasing α makes x to recover its maximum value more rapidly. The link weight effectively remains constant in practice if such a recovery becomes very fast, so that one sometimes speaks of "$\alpha = 0$" as the limit of static synapses which characterizes the standard Ising and Hopfield cases [36,37]. The origin of (5) are differential equations trying to account for the

fact that electrical stimulation due to local and even spatially extended activity may induce short-term plasticity leading to *depression* and sometimes also *facilitation* of synaptic transmission [35,38].

The relevant order in this system may be described by monitoring the firing rate, i.e., $m(t) = \frac{1}{N}\sum_i s_i(t)$, which is in fact sometimes recorded in laboratory experiments. Though hardly experimentally accessible, also interesting to illustrate in detail the system behavior is the overlap of the actual state with each pattern μ, defined as

$$m^{\mu}(t) = \frac{1}{Np(1-p)}\sum_{i=1}^{N}(\xi_i^{\mu} - p)s_i(t). \qquad (6)$$

Furthermore, we are interested in measuring the intensity of the input-output correlation, so that we shall compute the function

$$C_f = \lim_{\tau \to \infty} \frac{1}{\tau}\int_0^{\tau} m(t)\exp(ift)dt, \qquad (7)$$

i.e., the Fourier coefficient at frequency f of the output firing rate. The relevant correlation, to be denoted $C(T)$ in the following, is signal dependent, e.g., we define it in the cosinus case as the value of $C(f,T) \equiv |C_f|^2/A_0^2$ computed at the frequency of the input signal.

The phase diagram of the above model with $A(t) = 0 \ \forall t$ was examined before [28,29,31,32,39]. The most detailed study so far concerns the case in which x in (4) is interpreted as a stochastic variable with distribution inspired in (5) [31]. A main result in this case, which does not differ essentially from the present one, is its relevance to better understanding cooperative phenomena in several fields. In particular, tuning properly parameter values, the model exhibits familiar equilibrium phases, namely, a disordered high-T phase —corresponding to the *paramagnetic* phase in condensed matter— in which (the stationary values of) all the overlaps are practically zero, a low-T phase with conventional order —corresponding to *ferromagnetism*— in which the global activity converges with time towards one of the attractors $\{\xi_i^{\mu}\}$, so that it is often taken as a model example of associative memory, and a —say, *spin-glass*— phase in which convergence is towards a mixture of stored patterns. In addition, the system may be tuned to
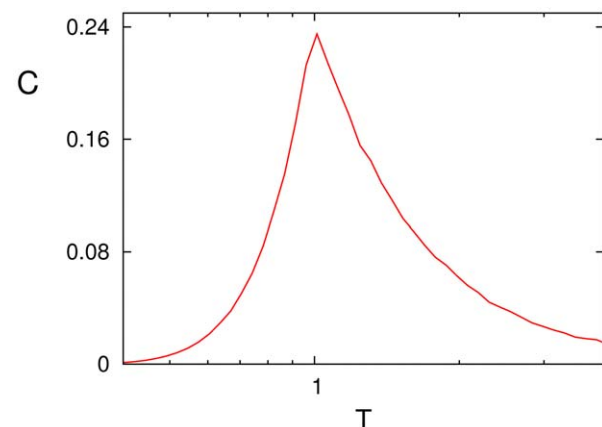

Figure 1. The signal–to–noise function $C(T)$ depicts in this semilogarithmic plot a shallow resonance for static synapses at the critical temperature. (Here, $A_0 = 0.005$, $f = 0.04$, and $p = 0.5$.)
doi:10.1371/journal.pone.0051170.g001

exhibit nonequilibrium phases [36]. Namely, (*i*) one in which there is a rapid and rather irregular roaming among the attractors — thus closely mimicking, for example, long-time structural changes and oscillations that have been associated with reaction–diffusion phenomena in physics and chemistry, as well as efficient, say, *states of attention* that are of interest in neuroscience—, (*ii*) one which is mainly characterized by oscillations between one of the stored patterns and its negative or corresponding *antipattern*, and (*iii*) one with quite irregular, apparently chaotic roaming randomly interrupted by pattern–antipattern oscillations [31]. The case (5) induces similar though relatively simpler behavior, e.g., the most involved behavior (*iii*) does not seem to fully develop in this case.

Results

From single to multiple resonance

We report here on Monte Carlo simulations of the above model. Exploratory runs showed no essential influence of N nor P in the main behavior of interest, so that we shall report first on the *sufficiently large*, typical case $N = 1000$, and will focus on $P = 1$, i.e., the only dynamic attractors are a given pattern and its antipattern. Varying N and P is also interesting, however, and we shall latter be concerned with this. The stored pattern will initially correspond to $p = 0.5$, which means same number of firing and silent neurons on the average, but changing p will be shown later on to modify importantly the system behavior. Time series for performing averages consisted of 10^5 Monte Carlo steps.

In the Hopfield limit of static synapses, $x(t) = 1$ $\forall t$, the system exhibits a rather weak resonance. As shown in Fig. 1, a well-defined though shallow peak in the input-output correlation occurs
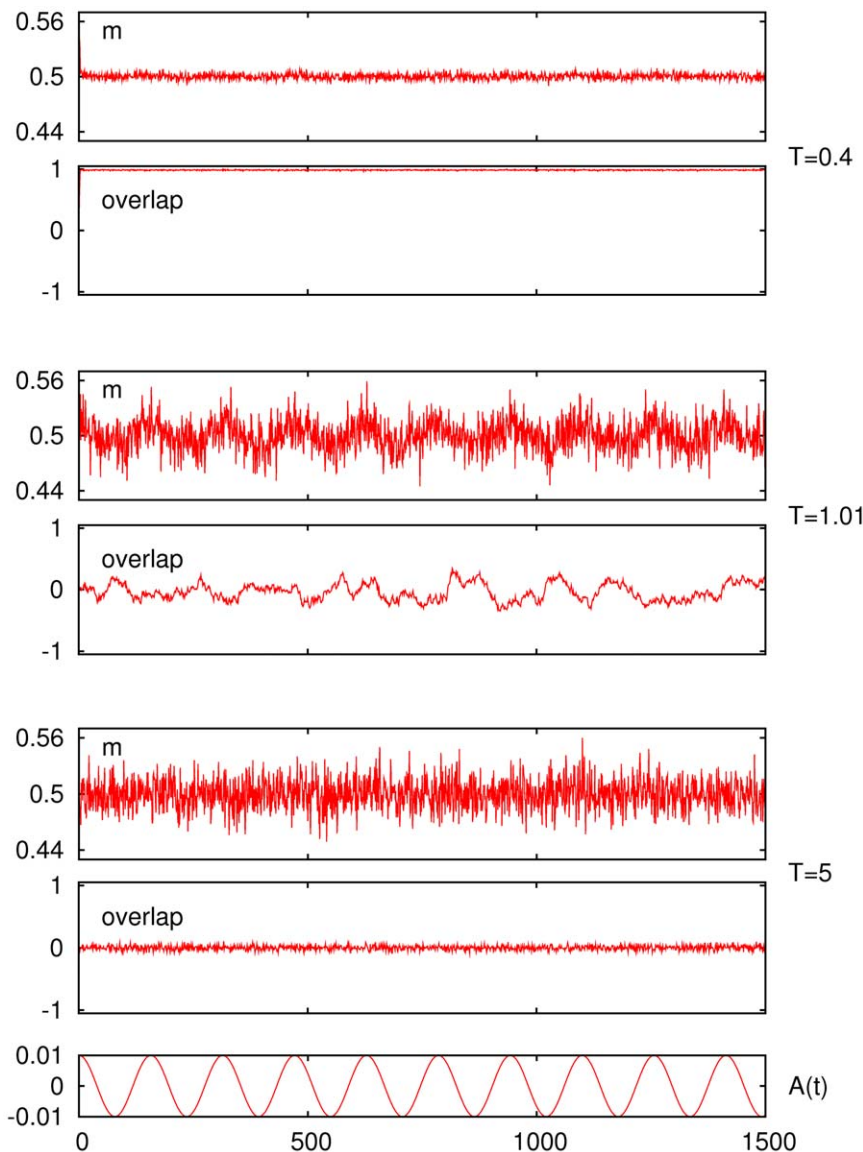

Figure 2. Three sets — at different noise level or *temperature* T, as indicated — each with two time series for, respectively, the firing rate (top of each set) and the overlap (bottom of each set) showing a tendency towards coherence at $T_C = 1$. The common external signal $A(t)$ and time scale are shown at the bottom below the sets. (Same case as in Fig. 1, except that $A_0 = 0.01$.)
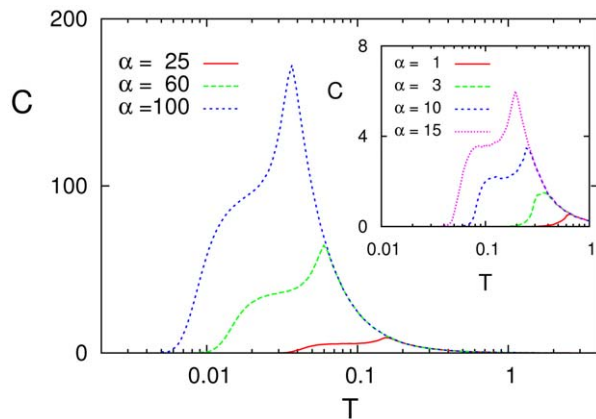doi:10.1371/journal.pone.0051170.g002

Figure 3. Different resonance curves $C(T)$ as one modifies the value of α in (5), as indicated, for $A_0 = 0.001$, $f = 0.04$ and $\beta = 0.5$.
doi:10.1371/journal.pone.0051170.g003

around $T = T_C = 1$. This is the bath temperature separating the ferromagnetic phase, for $T < T_C$, from the disordered phase, for $T > T_C$. The mechanism behind this behavior is illustrated in Fig. 2. This exhibits typical time series corresponding to the two relevant equilibrium phases. Namely, one is characterized by non-zero overlap —in fact, this is close to its maximum in our example shown as the second graph of the top set for $T = 0.4$— and the other by zero overlap —i.e., small-amplitude fluctuations around zero as in the bottom set. This figure also exhibits a near-critical condition (middle set) in which the overlap shows larger-amplitude fluctuations. It is remarkable that only in the latter case with $T \approx T_C$ is the firing rate clearly coupled to the cosinus within $A(t)$; the overlap also happens to be somewhat coupled here to the signal but this is not obvious to the naked eye in Fig. 2. The familiar critical bistability resulting from a competition between *thermal* fluctuations and —static though non-homogeneous— node interactions is in this case the mechanism [18,19] that allows the weak signal to prevail despite the noise.

More involved behavior shows up when synapses are dynamic, namely, x in (4) varies with time as stated in (5). As a matter of fact, one may then expect changes in the transmission of signals, given the very different development of order which occurs depending
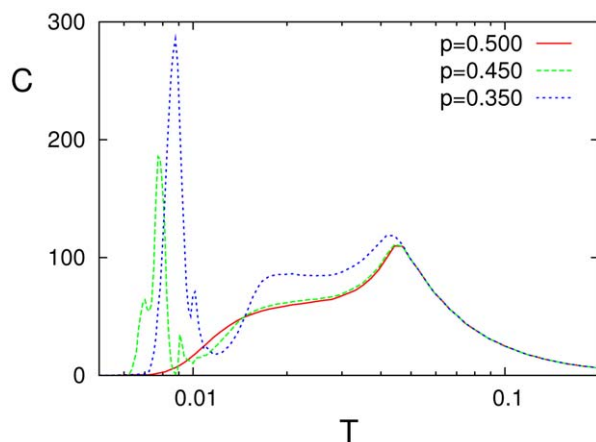

Figure 4. Resonance curves when one introduces an essential asymmetry by varying the mean neuron activity in the stored pattern, p, as indicated. (Here, $A_0 = 0.001$, $f = 0.04$, $\beta = 0.5$ and $\alpha = 80$.)
doi:10.1371/journal.pone.0051170.g004

on the parameter values in this case, as we described at the end of the previous section.

Fig. 3 illustrates the case as one modifies the depression parameter α in (5). The SR maximum is still clearly depicted for any α, but it corresponds now to the transition between the equilibrium disordered phase and the nonequilibrium one characterized by (possibly irregular) oscillations of the global activity —that is, the phase identified (ii) above. Furthermore, two other main differences arise. One is that the peak location moves as α increases towards lower temperature, in agreement with a reported scaling of the critical temperature with synaptic depression [28]. Furthermore, there is a factor of near 10^3 in the vertical scale here as compared to the one in Fig. 1, namely, the resonance effect is now much stronger, though the signal for this figure is even weaker than in the simulation before for static synapses.

Actually more intriguing is some indication of SMR for dynamic synapses, i.e., $C(T)$ tends to form and sometimes develops a plateau at low temperature which seems to announce a second resonance peak having a different origine that will finally show up for $p \neq 0.5$. The tendency is not fully materialized here, however, due to our restriction so far to strictly symmetric patterns ($p = 0.5$), which induces some symmetry of the connection intensities, as we discuss next.

Effects of asymmetry

The fact that the incipient correlation plateaus in Fig. 3 are associated to the mechanisms inducing transitions between the equilibrium-memory and nonequilibrium-oscillatory phases is confirmed by analysis of the corresponding time series (not shown). That is, one observes that the overlap then describes rapid oscillations between the stored pattern and its antipattern that are definitely correlated with the signal waving. Closer inspection does not evidence any such correlations in the firing rate series, however. Consequently, the function $C(T)$ —which derives from $m(t)$— shows no definite peak. This apparent inconsistency is because, in as long as one considers $p = 0.5$, the firing rate, unlike the overlap, fluctuates with only small amplitude, around $m = 0.5$ in practice. It follows that analyzing $p \neq 0.5$ is needed now, specially after one notices that the asymmetric case is in fact the only bearing interest for hypothetical realizations of this resonance phenomenology in the laboratory.

Figs. 4 and 5 illustrate the change of behavior as the mean neuron activity in the pattern, p, is modified. The first one shows that any asymmetry in the number of firing and silent neurons induces SMR, namely, a sharp peak (together with some "harmonics") at very low T, near the transition between memory and oscillatory phases, and a cleaner and somewhat less pronounced peak at higher T, near the transition between oscillatory and disordered phases. Interesting enough, the resonance is enhanced with increasing asymmetry. We also notice that, as expected, the underlying pattern-antipattern symmetry induces the same behavior for $p > 0.5$ than for $p < 0.5$.

Fig. 5 clearly depicts the nature of the low-temperature resonance peak and how this is associated with asymmetry. That is, the oscillations of the firing rate are essentially different for the two cases of correlated behavior. One observes at $T = 0.045$ a behavior that resembles the one for the middle set in Fig. 2. This is a critical condition, corresponding to a second–order phase transition, in which the resonance is essentially induced by noise and long–ranged correlations. There are oscillations of both $m(t)$ and $m^\mu(t)$ that are definitely correlated with those of $A(t)$ —which results in the high-T resonance peak— but occurring between states that, due to the underlaying noise, are not strongly

correlated with the information content, as one should have expected given that jumping is now practically among the store pattern and a disordered phase. Perhaps the most striking observation here is that $m^\mu(t)$ subtly correlates with the signal, namely, it occurs as a modulation in the amplitude of the pattern–antipattern oscillations (see middle panel of the bottom left set in Fig. 5). Also interesting is that, in spite of the noise in this case, the weak signal is able to correlate with the neurons activity therefore affecting the processing of information at very short time scales, as discussed further in the next section.

The relevant mechanism happens to be qualitatively different near the low-T resonance peak, e.g. $T = 0.0076$ in Fig. 5. Both the firing rate and the overlap now show abrupt oscillations with precisely the same frequency and strongly correlated with $A(t)$. In

particular, the low (high) firing metastable states corresponding to high (low) overlap —i.e., transitions between the two only possible levels of neural activity in the (normal) case of asymmetric patterns— are synchronized to the maxima (minima) of the cosinus signal. As in a first–order phase transition, and unlike the high-T case, such a strong correlation tends to diminish sharply as T is either increased or decreased even slightly, Fig. 5 reveals. Furthermore, none of the time series, $m(t)$ and $m^\mu(t)$, display superimposed fluctuations, confirming that the noise, even though necessary, is not here the relevant cause. The control is now in the weak signal, and the global activity changes correlated with the information content during a relatively long time, namely, one at least of order of the signal period.
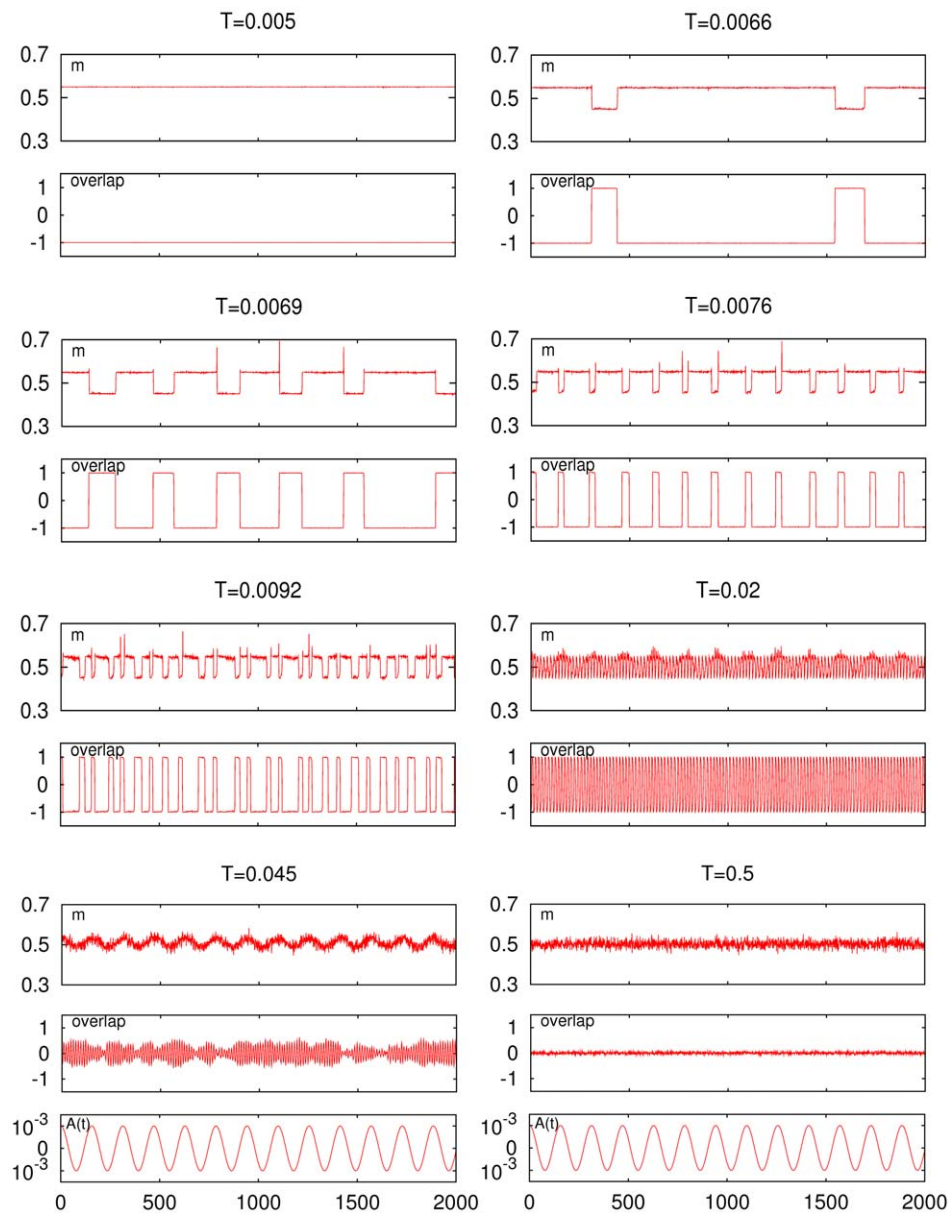

Figure 5. Time series for the firing rate (top graph of each set) and for the overlap (bottom graph of each set) at different temperature, as indicated, in the asymmetric case $p = 0.45$**.** (Other parameters as in Fig. 4.) The second set from top in the right column corresponds to the low-T peak; the bottom set in the left column corresponds to the high-T peak. The common external signal $A(t)$ and time scale are shown at the bottom below the sets.
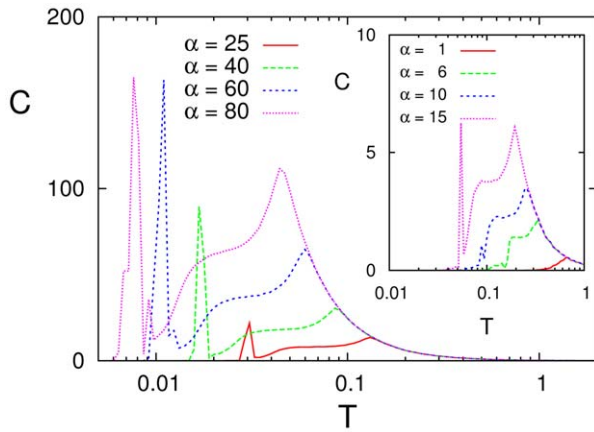doi:10.1371/journal.pone.0051170.g005

Figure 6. Resonance curves for varying α, **as indicated, when** $p = 0.45$ **and** $\beta = 0.5$, **for a sinusoidal signal with** $A_0 = 0.001$ **and** $f_0 = 0.04$.
doi:10.1371/journal.pone.0051170.g006

Figure 7. Effect of varying the amplitude A_0 **for** $p = 0.45$. The inset shows the dependence on A_0 of the amplitude of the oscillations of $m(t)$ for each of the two peaks.
doi:10.1371/journal.pone.0051170.g007

Fig. 6 illustrates the situation for $p \neq 0.5$ as one changes α. On one hand, the behavior happens to be similar to the one for SR as observed above in the symmetric case (cf. Fig. 3), namely, increasing (decreasing) α shifts the peaks to lower (higher) T and, at the same time, the high of the peak increases (decreases). On the other hand, the two peaks tend to merge into a single one as α is decreased, and the low-T peak does not really show up in practice for any $\alpha < 10$. A main conclusion is therefore that SMR requires both asymmetry of the patterns concerning p in (1), which is in fact a general property of nature, and large enough values of the parameter α characterizing the synaptic changes in (5), i.e., a complex functionality of connections —even though the actual wiring may be a simple, fully-connected one.

Changing the signal

The above suggests that the details of the input signal may also have an effect on resonance. Indeed, Fig. 7 reveals a substantial influence of the amplitude A_0, and confirms the different nature of the two peaks. While the high-T peak remains constant, the low-T peak strongly increases with A_0 for $p \neq 0.5$. This is due to the normalization of $C(T)$ with respect to A_0. That is, since the oscillations that correspond to the first peak are fixed in amplitude (the system is switching between pattern and antipattern), the normalization factor leads to the inverse dependence between the peak height and the signal amplitude. This is not the case for the second resonance peak because the amplitude of the oscillations in the firing rate also increases with A_0. This peak of C thus remains constant, maintaining its shape and height independently of the value for A_0. Such differences are a consequence of what we observed above in relation with Fig. 5. That is, the behavior around $T = 0.045$ is determined more by the signal —and, therefore, by A_0— than by the well to be overcome at the transition point, while the well depth dominates over the signal influence around the (first–order) transition in $T = 0.0076$.

We also checked the robustness of behavior in relation to the nature of the signal. Let us consider, which is a familiar case, a non-homogeneous Poissonian spike train with an instantaneous firing rate modulated by a slow sinusoidal function. That is, instead of a cosinus, we shall now use in Eq. (3) the signal $A(t) = A_0 \sum_{i=1}^{k} \delta(t - t_i)$ were the occurrence times t_i are generated from a non-homogeneous Poisson process of mean $\lambda(t) = \lambda_0[1 + a\cos(ft)]$, i.e., varying with time. This is believed to
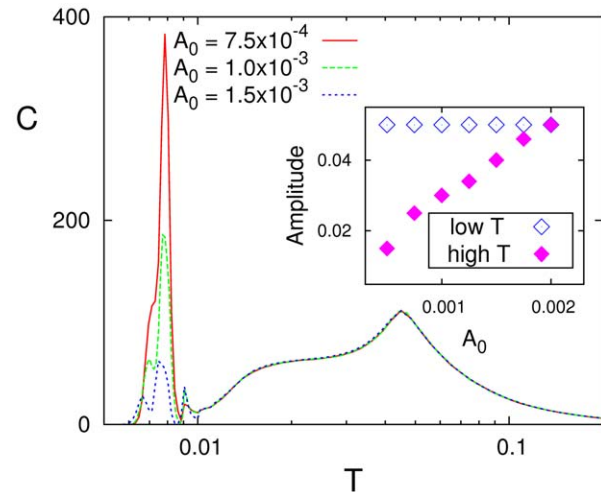
be more realistic than a sinus or a cosinus, at least for neural systems, e.g., this is sometimes assumed to represent the spike activity of a neuron in sensory areas processing structured external signals from senses. This choice is also a more general function, which eliminates specific features of the cosinus and includes both stochasticity (inherent here to the Poisson process) and some quasi–periodic structure codifying relevant information, which is important for the involved phenomena.

A first observation is that, as Fig. 8 illustrates, no essential qualitative changes occur using one or the other signal in a typical case of SMR. On the other hand, inspection of time series as those in Fig. 9 shows again indications of the different nature of the two peaks. At low T, e.g., $T = 0.007$ in this figure, the firing rate switches from low to high mean activity each time a train or burst of inputs arrives. Once the stimulus ends or the arriving signals become sparse, the system stays at the metastable state of high activity —as it occurs in Fig. 5 for the cosinus maxima— until synapses depress, due to such staying at high activity, and the metastable state destabilizes. It seems sensible to link this behavior with that in a hypothetical working memory context in which the activity persists for some time after the stimulus has ceased. As a matter of fact, a sort of short–term synaptic plasticity which reminds one of this situation has already been proposed [40,41]. On the contrary, the system processes without slothfulness at high T, e.g., $T = 0.045$ in Fig. 9. That is, a single spike input induces switching from low to high activity, and the high activity state persists but only during the duration of the stimulus, so that any temporal structure encoded in the signal is precisely processed at the high-T resonance.

Discussion

We here studied the origin of stochastic resonance as it occurs in a biologically-motivated Ising-Hopfield model system with thresholded neurons and dynamic synapses. This results in an interacting complex network, namely, one in which the intensity of connections is inhomogeneously distributed and varies with time, which essentially influences functionality. For a wide range of parameter values, the system shows intense resonance for different levels of noise. More specifically, as the noise is increased in case $P = 1$, i.e., when the system *stores* a single pattern, the network
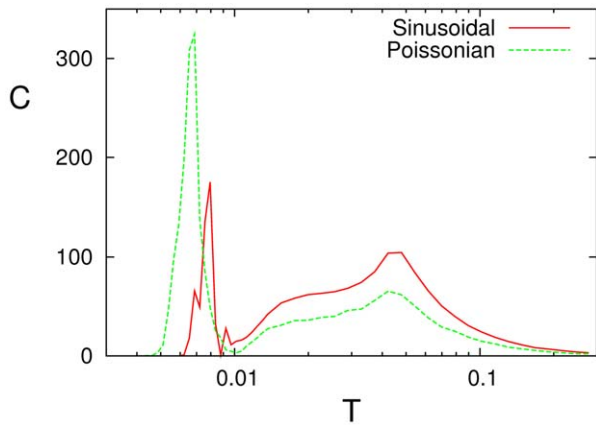
Figure 8. Resonance curves for a sinusoidal signal and for a non-homogeneous Poissonian input train (in this case, $C(T)$ stands for $|C_f|^2/A_0^2\lambda_0^2$ at the modulation frequency f of the non-homogeneous Poissonian process rate). Here, $p=0.45$, $\alpha=80$, $\beta=0.5$, $f=0.04$, and $A_0=0.001$ for the sinus and $A_0=0.005$, $\lambda_0=0.05$, and $a=0.75$ for the Poissonian signal.
doi:10.1371/journal.pone.0051170.g008

activity passes from a resting state with some activity around this pattern to a phase in which this situation destabilizes and the global activity oscillates between the metastable states corresponding to the pattern and its antipattern configurations. When the noise increases even more, the pattern–antipattern oscillations wash out and a disordered phase emerges. Interesting enough, SMR happens to require in this setting some synaptic depression, so that the relevant phases occur —and the stored pattern to be asymmetric as it is always the case in practice. Two resonance peaks —namely, sudden increase of the efficiency in transmitting a weak signal through two different levels of the environmental noise— are then exhibited that are associated with the transitions points between the phases.

The nature of the peaks importantly differs from each other. The low noise one is mainly due to the coupling between the frequency of the pattern–antipattern oscillations —associated to the occurrence of nonequilibrium phases— and the waving of the input signal. The high noise peak, however, ensues when a modulation of the amplitude of these oscillations (and not the pattern–antipattern oscillations themselves) correlates with the signal. This relevant modulation clearly manifests itself as a noisy slow oscillation in the firing rate, as illustrated by the inset of Fig. 7
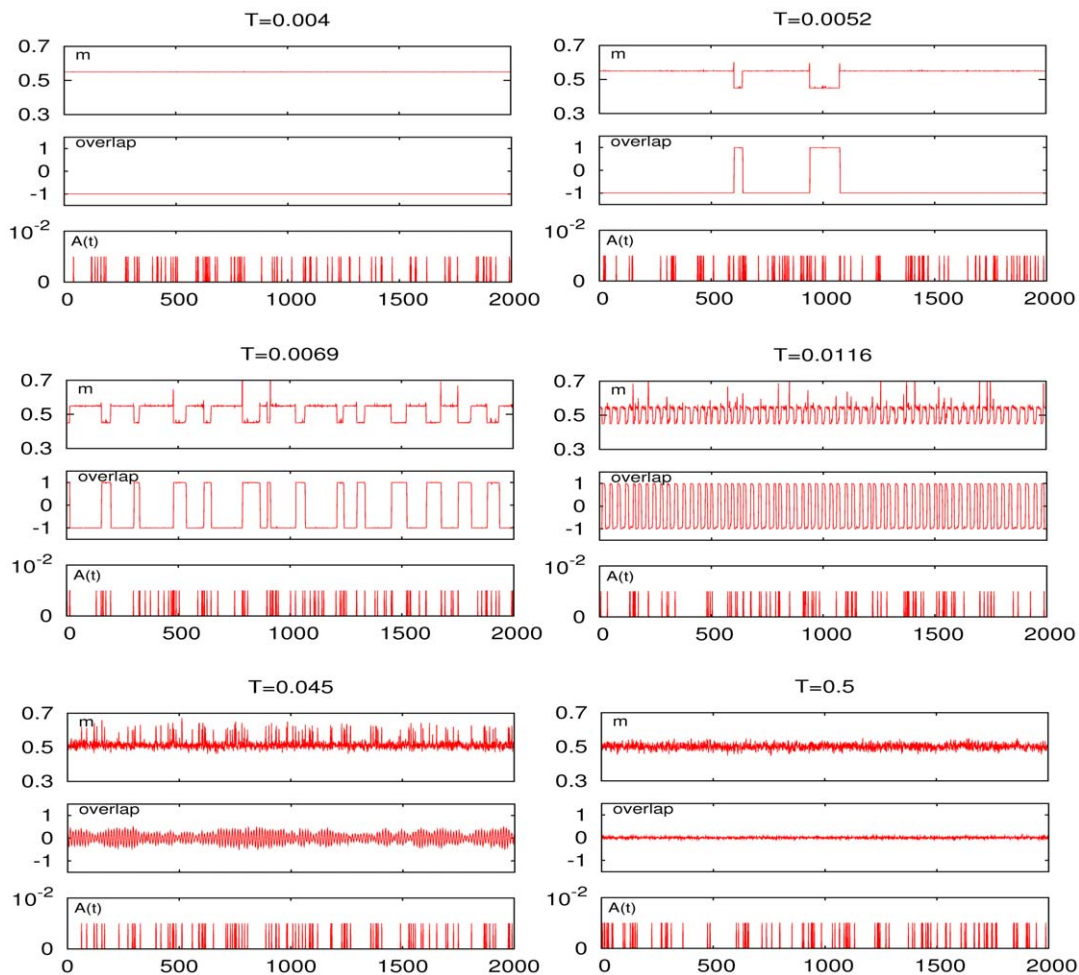

Figure 9. Time series for different values of T, as indicated, corresponding to the SMR curve in Fig. 8 for the Poissonian input train (shown below each set with the time scale). The resonances occur in this case around $T=0.007$ (second set in the left collumn) and $T=0.045$ (third set in the left collumn).
doi:10.1371/journal.pone.0051170.g009

showing how the amplitude of the firing rate oscillations increases with the amplitude of the signal.

The peaks not only differ in their birth mechanism but also in the way the signal is processed. This is made evident when an inhomogeneous Poissonian spike train of small amplitude is used as input signal. Around the low-noise peak, the system activity rather tends to follow the signal every time a burst of spikes arrives, and it remains excited for a time, which is short but larger than the stimulus duration, until the synaptic fatigue mechanism destabilizes such metastability. This is precisely the basic microscopic origin of peculiar properties reported to occur in nature such as undamped propagation in excitable media [4,32,33], and it may also be interpreted as a sort of short–term memory mechanism able to maintain information for, say, a few seconds as in the so–called sensory and working memories. The situation essentially changes around the high-noise peak, where the system detects each single input spike, that is, the finest time structure of the underlying signal.

We also checked how SMR is affected by varying the number P of stored patterns. This is interesting for completeness but also because the global activity becomes for $P > 1$ even more complex. That is, the system then tends to keep visiting all the stored patterns and their antipatterns, and it may do this by following quite irregular, even chaotic paths [31]. As Fig. 10 shows, increasing P for a fixed frequency f of the input signal (left), the high–noise resonance slightly increases and moves a little bit towards lower T, and the low-T peak markedly decreases while moving to lower T. This is due to the fact that increasing P tends to increase the frequency of the pattern–antipattern oscillations of the firing rate and, therefore, to decorrelate the firing rate from the input signal. This is as expected because the memory capacity of the standard Ising–Hopfield model is known to generally decrease due to interference among the stored patterns [42]. For a given value of P, on the other hand, the height of the low-noise peak increases with the frequency f of the signal as this approaches the frequency of the pattern–antipattern oscillations (right graph in Fig. 10). The net result is therefore that SMR is robust for a range of P values as far as input signals are of high frequency, while one should expect the low–frequency signals to be poorly processed.

A picture similar to the one in Fig. 1 was reported before in settings that are close to ours here but involving serious restrictive
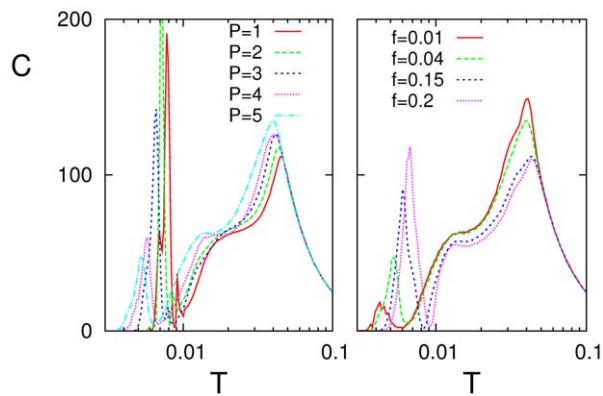

Figure 11. Effect of the network size N on SMR. The inset shows how the value of T locating the low (circles) and high (squares) noise peaks depends on N. This is for a sinusoidal signal with $A_0 = 0.001$ and $f_0 = 0.04$, and $p = 0.45$, $\alpha = 80$ and $\beta = 0.5$.
doi:10.1371/journal.pone.0051170.g011

conditions [43–45]. In particular, a recent study within the linear and mean-field approximations of the Ising model with — constant and homogeneous — ferromagnetic interactions under an oscillating magnetic field [44,45] describes resonance behavior when the wiring of connections is not homogeneous. The outcome happens to depend crucially on specific properties of the involved network structure, and the resonance resembles the one in Fig. 1 when the degree distribution obeys a power law $\sim k^{-\gamma}$ with $\gamma > 3$. In spite of its interest for other purposes [46–48], the relevance of the Ising model on scale-free networks is perhaps questionable within the present context. That is, large values of γ are generally not observed in nature, and the system is physically anomalous due to finite-size effects for $2 < \gamma < 3$ [44–48]. On the contrary, it is remarkable in our model that defining its wiring a situation in which all neurons are in principle connected to each other, the

Figure 10. Left: Resonance curves for $f = 0.04$ as the number P of stored patterns is varied, suggesting that the low-T resonance tends to disappear with increasing P. Right: Resonance curves for $P = 5$ as one varies the signal frequency f. This shows the contrary effect, i.e., the low-T resonance intensity increases with f. (Here, $p = 0.45$, $A_0 = 0.001$, $\alpha = 80$, and $\beta = 0.5$).
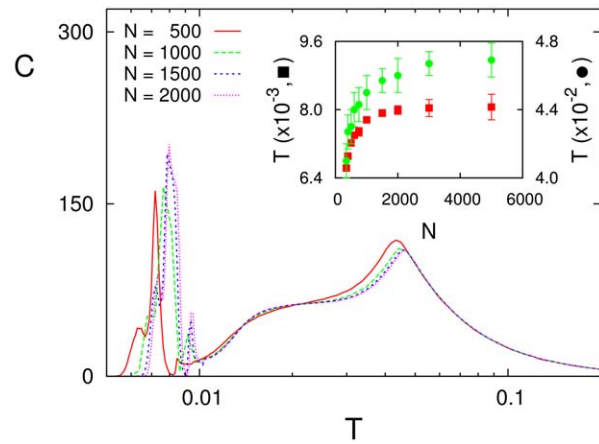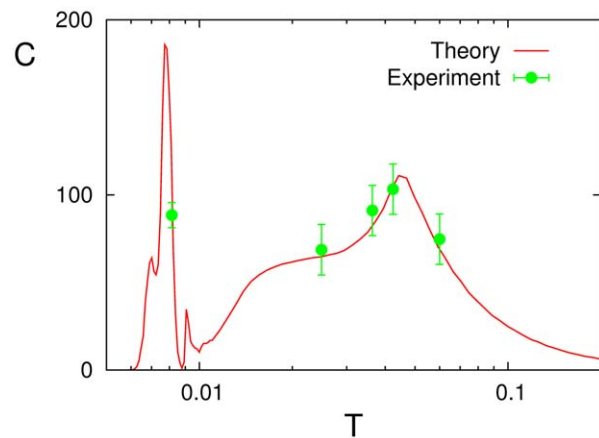doi:10.1371/journal.pone.0051170.g010

Figure 12. The experimental data (symbols with the corresponding error bars) reported in [54] are plotted here against our theoretical prediction (red solid line) corresponding to the case $p = 0.45$ in Fig. 4. To obtain this fit, the experimental data C with arbitrary units are multiplied by a factor 180, and the external noise amplitude N (which is given in dB) needed to be transformed into our intrinsic noise parameter T using the nonlinear relationship $T = 10^{-4} \{ T_0 + \frac{\eta N}{2} [1 + \mathrm{erf}((N - N_0)/\sqrt{2}\sigma_N)] \}$ with $T_0 = 5$, $\eta = 7.7$, $N_0 = 50$dB, and $\sigma_N = 26.19$dB.
doi:10.1371/journal.pone.0051170.g012

intensity of connections is not homogeneous and constantly varies with time. This in fact induces a real complex functionality of the network which is likely to correspond more generally to the one in nature [49–53].

Fig. 11, on the other hand, shows how the results in this paper do not depend essentially on the network size N. That is, SMR occurs qualitatively the same for a range of sizes, and the value of noise at which the peaks develop depends on N but tends soon to saturate at a constant value. This is interesting because the neural systems that we attempt to describe are far from being *infinite* in the thermodynamic sense but correspond to relatively small values of N.

Finally, we comment on possible experimental realizations of SMR. Some limited data from a psychotechnical experiment [54–56] concerning the human cortex were recently interpreted in the light of SMR using a simple model consisting of FitzHugh–

Nagumo neurons [57–60], which account for adaptive thresholds and fatigue–enduring synapses [21]. This in fact motivated the present study of a similar situation in a complex network. We therefore attempted a new contact between those experimental data and the present model; figure 12 shows the result, which is encouraging. No doubt that further experiments trying to confirm SMR, which will thus clarify the possible existence of intriguing mechanisms as suggested by the model in this paper, will be most welcome.

Author Contributions

Conceived and designed the experiments: JJT JM GP. Performed the experiments: GP. Analyzed the data: GP JJT JM. Wrote the paper: JM JJT GP.

References

1. Golyandina N, Nekrutkin V, Zhigljavsky A (2001) Analysis of Time Series Structure: SSA and Related Techniques. CRC Press.
2. Dimova II, Kolma PN, Maclina L, Shibera DYC (2012) Hidden noise structure and random matrix models of stock correlations. Quantive Finance 12: 567–572.
3. Sagués F, Sancho JM, García-Ojalvo J (2007) Spatiotemporal order out of noise. Rev Mod Phys 79: 829–882. See also, for instance, "René Descartes on snowflakes", supplemental material for Furukawa Y, Wettlaufer JS (2007) Snow and ice crystals. Physics Today 60: 70–71.
4. Jung P, Mayer-Kress G (1995) Spatiotemporal stochastic resonance in excitable media. Phys Rev Lett 74: 2130–2133.
5. Lindner B, Garca-Ojalvo J, Neiman A, Schimansky-Geier L (2004) Effects of noise in excitable systems. Physics Reports 392: 321–424.
6. Benzi R, Sutera A, Vulpiani A (1981) The mechanism of stochastic resonance. J of Phys A: Math and Gen 14: L453.
7. Wiesenfeld K, Moss F (1995) Stochastic resonance and the benefits of noise: from ice ages to crayfish and squids. Nature 373: 33–36.
8. Anishchenko VS, Neiman AB, Moss F, Shimansky-Geier L (1999) Stochastic resonance: noiseenhanced order. Physics-Uspekhi 42: 7–36.
9. Krawiecki A, Holyst JA (2003) Stochastic resonance as a model for financial market crashes and bubbles. Physica A 317: 597–608.
10. Munakata T, Sato AH, Hada T (2005) Stochastic resonance in a simple threshold system from a static mutual information point of view. J Phys Soc Japan 74: 2094–2098.
11. Sato AH (2006) Frequency analysis of tick quotes on foreign currency markets and the doublethreshold agent model. Physica A 369: 753–764.
12. McDonell MD, Stocks NG, Pearce CEM, Abbott D (2008) Stochastic Resonance: From Suprathreshold Stochastic Resonance to Stochastic Signal Quantisation. Cambridge University Press.
13. Special issue "Stochastic resonance" (2009) Eur Phys J B 69:1.
14. Ghosh PK, Marchesoni F, Savel'ev SE, Nori F (2010) Geometric stochastic resonance. Phys Rev Lett 104: 020601.
15. Tuckwell HC, Jost J (2012) Analysis of inverse stochastic resonance and the long-term firing of hodgkin-huxley neurons with gaussian noise. Submitted, arXiv:1202.249.
16. Weaver RL, Lobkis OI (2001) Ultrasonics without a source: Thermal fluctuation correlations at mhz frequencies. Phys Rev Lett 87: 134301.
17. Snieder R, Wapenaar K (2010) Imaging with ambient noise. Physics Today 63: 44–49.
18. McNamara B, Wiesenfeld K (1989) Theory of stochastic resonance. Phys Rev A 39: 4854–4869.
19. Gammaitoni L, Marchesoni F, Menichella-Saetta E, Santucci S (1989) Stochastic resonance in bistable systems. Phys Rev Lett 62: 349–352.
20. Fulinski A, Gra PF (2000) Universal character of stochastic resonance and a constructive role of white noise. J Stat Phys 101: 483–493.
21. Torres JJ, Marro J, Mejias JF (2011) Can intrinsic noise induce various resonant peaks? New J of Physics 13: 053014.
22. Vilar JMG, Rubí JM (1997) Stochastic multiresonance. Phys Rev Lett 78: 2882–2885.
23. Kim BJ, Minnhagen P, Kim HJ, Choi MY, Jeon GS (2001) Double stochastic resonance peaks in systems with dynamic phase transitions. EPL 56: 333.
24. Hong H (2005) Enhancement of coherent response by quenched disorder. Phys Rev E 71: 021102.
25. Barbi M, Reale L (2005) Stochastic resonance in the lif models with input or threshold noise. Biosystems 79: 61–66.
26. Tessone CJ, Mirasso CR, Toral R, Gunton JD (2006) Diversity-induced resonance. Phys Rev Lett 97: 194101.
27. Zhang J, Liu J, Chen H (2008) Selective effects of noise by stochastic multi-resonance in coupled cells system. Sci China Ser G 51: 492–498.
28. Pantic L, Torres JJ, Kappen HJ, Gielen SCAM (2002) Associative memory with dynamic synapses. Neural Comput 14: 2903–2923.
29. Torres JJ, Cortes JM, Marro J, Kappen HJ (2008) Competition between synaptic depression and facilitation in attractor neural networks. Neural Comput 19: 2739–2755.
30. Mejias JF, Hernandez-Gomez B, Torres JJ (2012) Short-term synaptic facilitation improves information retrieval in noisy neural networks. EPL 97: 48008.
31. de Franciscis S, Torres JJ, Marro J (2010) Unstable dynamics, nonequilibrium phases, and criticality in networked excitable media. Phys Rev E 82: 041105.
32. Marro J, Torres JJ, Cortes JM (2008) Complex behavior in a network with time-dependent connections and silent nodes. J Stat Mech 2008: P02017.
33. Torres JJ, Marro J, Cortes JM, Wemmenhove B (2008) Instabilities in attractor networks with fast synaptic fluctuations and partial updating of the neurons activity. Neural Networks 21: 1272–1277.
34. Sejnowski TJ (1977) Storing covariance with nonlinearly interacting neurons. J Math Biol 4: 303–321.
35. Tsodyks MV, Markram H (1997) The neural code between neocortical pyramidal neurons depends on neurotransmitter release probability. Proc Natl Acad Sci USA 94: 719–723.
36. Marro J, Dickman R (1999) Nonequilibrium Phase Transitions in Lattice Models. Cambridge University Press.
37. Hopfield JJ (1982) Neural networks and physical systems with emergent collective computational abilities. Proc Natl Acad Sci USA 79: 2554–2558.
38. Jimbo Y, Tateno T, Robinson HP (1999) Simultaneous induction of pathway-specific potentiation and depression in networks of cortical neurons. Biophys J 76: 670–678.
39. Cortes JM, Torres JJ, Marro J, Garrido PL, Kappen HJ (2006) Effects of fast presynaptic noise in attractor neural networks. Neural Comput 18: 614–633.
40. Hempel CM, Hartman KH, Wang XJ, Turrigiano GG, Nelson SB (2000) Multiple forms of shortterm plasticity at excitatory synapses in rat medial prefrontal cortex. J Neurophysiol 83: 3031–3041.
41. Mongillo G, Barak O, Tsodyks M (2008) Synaptic theory of working memory. Science 319: 1543–1546.
42. Amit DJ (1989) Modeling brain function: the world of attractor neural network. Cambridge University Press.
43. Brey JJ, Prados A (1996) Stochastic resonance in a one-dimensional ising model. Physics Letters a 216: 240–246.
44. Krawiecki A (2008) Stochastic multiresonance in the ising model on scale-free networks. Acta Phys Polonica B 39: 1103–1114.
45. Krawiecki A (2009) Structural stochastic multiresonance in the ising model on scale-free networks. Eur Phys J B 69: 81–86.
46. Torres JJ, Munoz MA, Marro J, Garrido PL (2004) Influence of topology on the performance of a neural network. Neurocomputing 58–60: 229–234.
47. Johnson S, Marro J, Torres JJ (2008) Functional optimization in complex excitable networks. EPL 83: 46006.
48. de Franciscis S, Johnson S, Torres JJ (2011) Enhancing neural-network performance via assortativity. Phys Rev E 83: 036114.
49. Eguíluz VM, Chialvo DR, Cecchi GA, Baliki M, Apkarian AV (2005) Scale-free brain functional networks. Phys Rev Lett 94: 018102.
50. Honey CJ, Ktter R, Breakspear M, Sporns O (2007) Network structure of cerebral cortex shapes functional connectivity on multiple time scales. Proceedings of the National Academy of Sciences 104: 10240–10245.
51. Petermann T, Thiagarajan TC, Lebedev MA, Nicolelis MAL, Chialvo DR, et al. (2009) Spontaneous cortical activity in awake monkeys composed of neuronal avalanches. Proceedings of the National Academy of Sciences 106: 15921–15926.
52. Friedman N, Ito S, Brinkman BAW, Shimono M, DeVille REL, et al. (2012) Universal critical dynamics in high resolution neuronal avalanche data. Phys Rev Lett 108: 208102.
53. Radicchi F, Baronchelli A, Amaral LAN (2012) Rationality, irrationality and escalating behavior in lowest unique bid auctions. PLoS ONE 7: e29910.

54. Yasuda H, Miyaoka T, Horiguchi J, Yasuda A, Hanggi P, et al. (2008) Novel class of neural stochastic resonance and error-free information transfer. Phys Rev Lett 100: 118103.

55. Lugo E, Doti R, Faubert J (2008) Ubiquitous crossmodal stochastic resonance in humans: Auditory noise facilitates tactile, visual and proprioceptive sensations. PLoS ONE 3: e2860.

56. Colgin LL, Denninger T, Fyhn M, Hafting T, Bonnevie1 T, et al. (2009) Frequency of gamma oscillations routes flow of information in the hippocampus. Nature 462: 353–357.

57. FitzHugh R (1961) Impulses and physiological states in theoretical models of nerve membrane. Biophys J 1: 445–466.

58. Nagumo J, Arimoto S, Yoshizawa S (1962) An active pulse transmission line simulating nerve axon. Proceedings of the IRE 50: 2061–2070.

59. Izús GG, Deza RR, Wio HS (1998) Exact nonequilibrium potential for the fitzhugh-nagumo model in the excitable and bistable regimes. Phys Rev E 58: 93–98.

60. Izhikevich EM (2007) Dynamical Systems in Neuroscience: The Geometry of Excitability and Bursting. The MIT Press.